

Article

# Experimental Identification and Vibration Control of A Piezoelectric Flexible Manipulator Using Optimal Multi-Poles Placement Control

Junqiang Lou <sup>1</sup>, Jiangjiang Liao <sup>1</sup>, Yanding Wei <sup>2,\*</sup>, Yiling Yang <sup>2</sup> and Guoping Li <sup>1</sup>

<sup>1</sup> College of Mechanical Engineering and Mechanics, Ningbo University, Ningbo 315211, China; LOUJUNQIANG@NBU.EDU.CN (J.Lou); neverstop2008@126.com (J.Liao); liguoping@nbu.edu.cn (G.L.)

<sup>2</sup> China Key Laboratory of Advanced Manufacturing Technology of Zhejiang Province, School of Mechanical Engineering, Zhejiang University, Hangzhou 310027, China; yangyiling@nbu.edu.cn

\* Correspondence: weiyd@nbu.edu.cn; Tel.: +86-0571-8795-3851

Academic Editors: Gangbing Song and César M. A. Vasques

Received: 6 January 2017; Accepted: 17 March 2017; Published: 21 March 2017

**Abstract:** This paper presents experimental identification and vibration suppression of a flexible manipulator with piezoelectric actuators and strain sensors using optimal multi-poles placement control. To precisely identify the system model, a reduced order transfer function with relocated zeros is proposed, and a first-order inertia element is added to the model. Comparisons show the identified model match closely with the experimental results both in the time and frequency domains, and a fit of 97.2% is achieved. Based on the identified model, a full-state multi-poles placement controller is designed, and the optimal locations of the closed loop poles are determined where the move distance of the closed loop poles is the shortest. The feasibility of the proposed controller is validated by simulations. Moreover, the controller is tested for different locations of the closed loop poles, and an excellent performance of the optimal locations of the closed loop poles is shown. Finally, the effectiveness of the proposed controller is demonstrated by experiments. Results show that the vibrations of the expected modes are significantly diminished. Accordingly, multi-mode vibrations of the manipulator are well attenuated.

**Keywords:** experimental identification; multi-poles placement control; piezoelectric flexible manipulator; active vibration control

## 1. Introduction

In the fields of aerospace, robotics, civil engineering and other industries, flexible structures are prevailing due to their advantages of lightweight and lower energy consumption. However, flexible structures are highly resonant systems and exhibit the inherent property of vibration in presence of external disturbances, which leads to a deterioration of positioning accuracy and efficiency. Thus, vibration suppression of those multi-mode structures becomes imperative [1]. In recent years, smart materials have been extensively used for vibration control of flexible structures. Those materials include shape memory alloys, piezoelectric transducers and so on [2]. Among them, piezoelectric materials have the advantages of small volume, fast response and can be easily integrated onto the host structures. As a result, active vibration control of smart structures utilizing piezoelectric materials has become more attractive [3].

To obtain a better performance for vibration suppression of flexible structures, both accurate dynamic modeling and suitable controller design are required. Controller design often relies on accurate modeling of the system dynamics [4]. In most previous studies, various efficient approaches have been proposed to establish the mathematical model of smart flexible structures. In general,

dynamic behaviors of flexible structures can be obtained by analytical modeling based on partial differential equations (PDEs) [5]. However, it is difficult to simulate the properties of a relatively complicated system accurately. In some cases, it is intractable, even impossible, to find the system differential equations. In addition, the introduction of piezoelectric actuators/sensors adds complexity to the analytical modeling. Numerical approaches based on finite element method (FEM) are developed to obtain equivalent finite-dimensional models of smart structures, and yield fairly accurate results [6]. However, these approaches always require intensive mathematical derivations, which are usually labor intensive and time consuming. Meanwhile, these modeling techniques are sometimes hindered by factors such as the assumption of ideal boundary conditions, perfect bonding between the host and actuators/sensors, and so on [7].

An alternative modeling approach is system identification, which captures the input-output dynamics of smart structures using experimental data. Moreover, the issues of the sensor/actuator dynamics, signal conditioners and control unit are all included in the experimental model. Thus, the established model faithfully represents the dynamics of the flexible structures incorporated with smart materials, and the tangled mathematic calculations are also avoided. The identification process can be conducted in the frequency domain, or in the time domain. Among those time domain methods, Bu et al. [8] presented an experimental model of a flexible beam system incorporated with piezoceramic actuators based on the ARMAX (auto-regressive moving average exogenous) model. Abreu et al. [9] derived a time-domain state space model of a flexible structure using the observer/Kalman filter identification method together with an eigensystem realization algorithm. Tavakolpour et al. [10] employed the genetic algorithm (GA) to identify the model parameters of a linear difference equation for a rectangular flexible plate system. Afshari et al. [11] utilized a prediction error method to obtain the ARMAX model of a flexible beam bonded with piezoceramic actuator/sensor, and implemented a model reduction method to find the amenable reduced order. Pradhan and Ubudhi [12] developed a nonlinear ARMAX model of a planar two-link flexible manipulator system, and designed a nonlinear adaptive controller based on the identified model. Flexible structures are distributed parameter systems, thus have multiple vibration modes, which display highly resonant behavior near to the structures' natural frequencies. For a vibration mode, the frequency and damping of the underlying sinusoidal behavior are the basic parameters to be estimated. San-Millan and Feliu [13] presented an algebraic derivative approach for online identification of the resonant frequencies of a flexible beam in the presence of noise and an offset. Qiu et al. [14] conducted an acceleration sensor based identification of modal frequencies for plate structures, including the first two bending and torsional modes. In order to estimate the model parameters of a flexible structure with collocated sensors/actuators, Bhikkaji et al. [15] proposed a novel frequency domain subspace identification scheme using the negative imaginary approach. To obtain the experimental model of a flexible plate, several frequency domain subspace identification algorithms with the instrumental variable idea were addressed by Ahmadzadeh et al. [16]. In addition, Orszulik and Shan [17] studied the application of the GA to identify the transfer function of a flexible manipulator system with collocated piezoelectric sensor/actuator.

Due to the inherent distributed nature, flexible structures have an infinite number of modes. However, it is impossible to model and active control all these modes due to the computational and control limitations. In practice, the reduced order models of flexible structures are always developed by modal truncation, where only the dominant modes are considered [18]. Consequently, the problem of spillover associated with the un-modeled but often non-negligible modes is unavoidable, and the spillover effect will cause instability of the closed loop system [19]. Although great progress has been achieved in the field of modeling of smart flexible structures, the issue is still far from completely solved.

Various studies have been conducted on the development and implementation of control algorithms for vibration suppression [20]. Classical feedback control strategies receive considerable attention as no adaptation time or reference signal is needed. Among those control methods, the poles placement method (PPM) is an effective approach for active vibration suppression despite its simplicity; it offers

users the possibility of placing the closed loop poles at some predetermined locations, which is desirable to set natural frequencies and damping ratios to specified values to achieve desired control performance [21]. Sethi and Song [22] applied the PPM for vibration control of the first dominant mode of flexible composite large I-beams, they further presented multi-mode vibration suppression of a cantilever beam using a poles placement controller with an observer [23]. Tehrani et al. [24] proposed a robust poles placement controller for structural vibration control using receptance data. Gordon and Erkorkmaz [25] studied the use of the poles placement technique to achieve active vibration damping and positioning control of ball screw drives. Tehrani et al. [26] developed a multi-input partial poles placement controller for vibration control of a glass-fiber beam using macro fiber composite (MFC) actuators. As the relocation of closed loop poles will alter the system stability characteristics and transient response, locations of the closed loop poles must be carefully determined.

The remainder of this paper is organized as follows. In Section 2, the experimental setup of the smart flexible manipulator system is introduced. In Section 3, a reduced order transfer function model with relocated zeros compensating for the neglect of higher modes is proposed. A first-order inertia element is added to the model. The system identification procedure is described, and the identified results are presented. The proposed poles placement method is described in Section 4. A method where the move distance of the closed loop poles is the shortest is proposed. To achieve desired damping characteristics of the target modes, only the real part of the dominant poles is adjusted. Thus, the natural frequencies of the structure are not affected. Simulations are conducted in Section 5. Subsequently, the experimental results and discussion are presented in Section 6. Conclusions are drawn in Section 7.

## 2. Experimental Setup

The experimental setup of the manipulator system is shown in Figure 1. The flexible manipulator used in this paper is a uniform aluminum cantilever beam and its properties are listed in Table 1. To fulfill the illustration of structural responses in the low frequency scope, instead of traditional PZT sensors, a full bridge strain gauge arrangement with the parameters detailed in Table 2, is attached on both sides of the beam as schematically illustrated in Figure 2. The strain gauge is chosen to lie near the root of the beam where the strain energy of the structure is the highest. Two PZT actuators with the properties listed in Table 3 are bonded onto both sides of the beam near the strain gauge. Moreover, a laser displacement sensor of Micro-Epsilon ILD 1402-50 (range: 50 mm, resolution: 5  $\mu$ m; Micro-Epsilon Messtechnik, Ortenburg, Germany) is used to measure the tip displacement of the manipulator. An electromagnetic vibrator (Sinocera Piezotronics INC, Yangzhou, China) is fixed to excite vibration of the beam as an external disturbance. The electromagnetic vibrator is located at 120.0 mm from the root of the beam. The real-time control system is implemented using a personal computer. A Data Acquisition (DAQ) device (National Instruments, Austin, OH, USA) of National Instrument PCI-6221(37 pin) is used for data acquisition and control output. The Lead zirconate titanate (PZT) actuator is driven by a power amplifier (Harbin Boshi Automation Co. LTD, Harbin, China), which can amplify the input signals from  $\pm 5$  V to  $\pm 75$  V. The strain signal is low-pass filtered and amplified through a strain amplifier, which can amplify the signal to a voltage range of  $\pm 10$  V. The output signal of the laser displacement sensor is conditioned to a voltage signal of 1–5 V by a signal conditioner. In addition, all the control algorithms are developed with the LabVIEW programming software (version 13.0, National Instruments, Austin, OH, USA).

**Table 1.** Properties of the manipulator.

Symbol	Quantity	Units	Value
$l_b$	length	mm	1070.2
$w_b$	width	mm	61.6
$t_b$	thickness	mm	2.1
$E_b$	Modulus of elasticity	Gpa	72
$\rho_b$	density	Kg/m <sup>3</sup>	2700

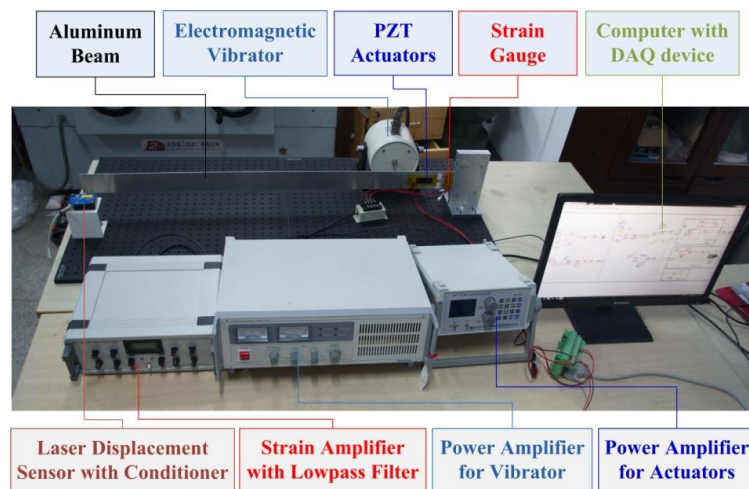


**Figure 1.** Experimental setup of the smart manipulator system. PZT: Lead Zirconate Titanate; DAQ: Data Acquisition.

**Table 2.** Properties of the strain measurement.

Symbol	Quantity	Units	Value
$S_g$	Gauge sensitivity	–	2.08
$R_s$	Resistance	$\Omega$	350
$K_s$	Amplification	–	5000
$U_o$	Supply Voltage	V	4.0
$x_s$	Location on the beam	mm	30.0

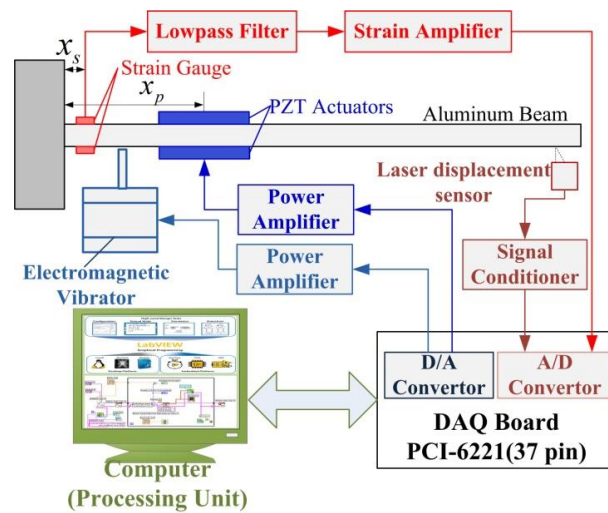


**Figure 2.** Block diagram of the experimental setup.

**Table 3.** Properties of the PZT patches.

Symbol	Quantity	Units	Value
$l_p \times w_p \times t_p$	Length $\times$ width $\times$ thickness	mm	$60 \times 20 \times 0.8$
$E_p$	Modulus of elasticity	Gpa	63
$\rho_p$	Patch density	$\text{kg/m}^3$	7650
$d_{31}$	Strain coefficient	C/N	$-166 \times 10^{-12}$
$x_p$	Location on the beam	mm	92.4

### 3. System Identification

System identification can be used to experimentally extract the dynamic model of a system. For system identification, a mathematical model of the beam is necessary. Due to the spatially distributed nature of flexible structures, it is highly desirable to work with transfer functions, thus the vibration dynamics of a cantilever beam can be written as Equation (1)

$$G(s) = k \sum_{n=1}^{\infty} \frac{1}{s^2 + 2\zeta_n \omega_n s + \omega_n^2} \quad (1)$$

where  $k$  is the gain of the open loop,  $n$  is the mode number,  $\zeta_n$  and  $\omega_n$  are the damping ratio and natural frequency of the  $n$ th mode, respectively. However, it is impractical to identify the infinite number of vibration modes. In practice, only a certain bandwidth is of interest, and dynamic response of the flexible structures is often dominated by the vibrations of the lower modes. Therefore, some form of mode truncation for the higher modes is needed. A common reduced order model used by Bhikkaji et al. [15] and Orszulik and Shan [17] is given as

$$G_c(s) = \sum_{i=1}^m \frac{k_i}{s^2 + 2\zeta_i \omega_i s + \omega_i^2} + D \quad (2)$$

where  $m$  is the number of modes kept in the model,  $k_i$  is the gain of the open loop for each mode, and  $D$  is a feedthrough term, which is added to compensate for the modal truncation effect. However, this neglect of higher modes still leads to the appearance of the direct energy transmission [27]. Therefore, the poles of the truncated system, which represent the resonance frequencies, are natural property of the system and independent among different modes, but the locations of the zeros will be distorted due to the omission of the higher modes. Besides, the PZT actuators are located a distance of 63.4 mm from the strain sensors, these locations may lead to sort of time delay. Above all, the truncated model with a pure delay element is given by Equation (3)

$$G(s) = ke^{-\tau s} \sum_{i=1}^m \frac{(s - a_i)(s - b_i)}{s^2 + 2\zeta_i \omega_i s + \omega_i^2} \quad (3)$$

where  $a_i$  and  $b_i$  are the relocated zeros of the  $i$ th mode due to the omission of the higher modes.  $\tau$  is the delay time.

Using Taylor series expansion, the pure delay element can be approximated as Equation (4)

$$e^{-\tau s} = \left[ \sum_{j=0}^{\infty} \frac{(\tau s)^j}{j!} \right]^{-1} = \left[ 1 + \tau s + \dots + \frac{(\tau s)^j}{j!} \dots \right]^{-1} \approx \frac{1}{1 + \tau s} \quad (4)$$

Then, the truncated model of the smart structure can be rewritten as Equation (5)

$$G(s) = \frac{k}{1 + \tau s} \sum_{i=1}^m \frac{(s - a_i)(s - b_i)}{s^2 + 2\zeta_i \omega_i s + \omega_i^2} \quad (5)$$

The pure delay element is approximated by a first-order inertia element as shown in Equation (5). Experiments were conducted to identify the parameters of the system model. A chirp signal with a frequency varies from 0.1 to 15 Hz was applied to the PZT actuators to have the chance of exciting the first two modes of the structure. The magnitude of the excitation signal was 5 V, and the identification experiment took 15 s. The sampling frequency was 200 Hz, and a low-pass filter was utilized with a cut-off frequency of 100 Hz. The time response signals for chirp excitation are plotted in Figure 3a,b.

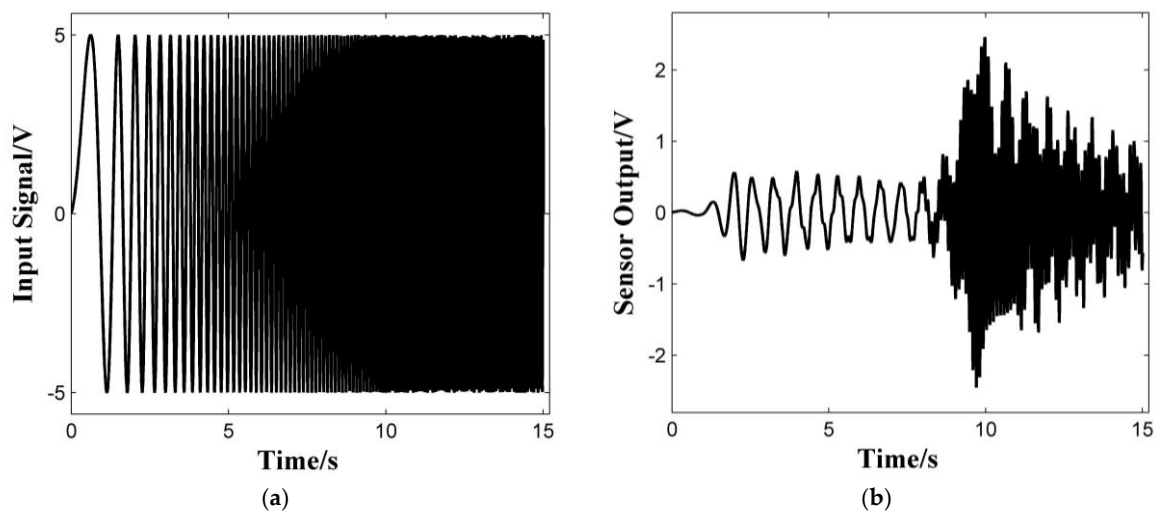


**Figure 3.** Time response of the chirp excitation and measured output signal: (a) chirp excitation signal; and (b) sensor output signal.

To find the transfer function of the system in the frequency domain, Fourier transform is performed on the chirp excitation signal  $u(t)$  and sensor output signal  $y(t)$ . The frequency response function (FRF) of the open loop system is given by Equation (6)

$$G(j\omega) = \frac{S_{uy}(j\omega)}{S_{uu}(j\omega)} \tag{6}$$

where  $S_{uy}(j\omega)$  is the cross spectral density between signal  $u(t)$  and  $y(t)$ , and  $S_{uu}(j\omega)$  is the auto spectral density of signal  $u(t)$ . The measured frequency response of the system is plotted in Figure 4. It can be seen that the natural frequencies of the first two modes of the smart structure are 1.47 and 9.06 Hz, respectively.

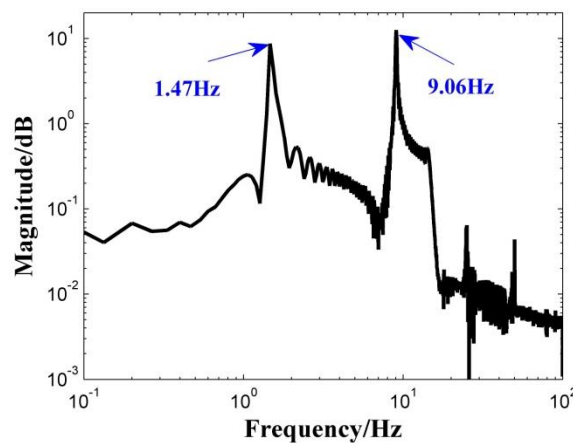


**Figure 4.** Measured frequency response of the system.

The system identification toolbox (Matlab software, version 7.0, Mathworks, Natick, MA, USA) was used for system identification. Based on Equation (5), the identified transfer function using the chirp signal is expressed as Equation (7). For comparison, the identified transform function depicted as Equation (2) is also given in Equation (8). The modal parameters for the two identified models are detailed in Table 4. Meanwhile, Bode diagram of the two identified transfer functions in the frequency range of interests (0.1–1000 rad/s) are plotted in Figure 5.

$$G(s) = \frac{13.44(s^2 + 0.72s + 6.66)(s^2 + 1.58s + 2045)}{(s + 355.4)(s^2 + 0.071s + 86.99)(s^2 + 0.42s + 3238)} \tag{7}$$

$$G_c(s) = \frac{-1.89}{s^2 + 0.071s + 87.05} + \frac{-43.69}{s^2 + 0.40s + 3238} + 0.035 \tag{8}$$

**Table 4.** Comparison of modal parameters for the identified models.

Model	Natural Frequencies		Damping Ratio	
	$f_1$	$f_2$	$\zeta_1$	$\zeta_2$
$G_c(s)$	1.48	9.06	0.004	0.004
$G(s)$	1.48	9.06	0.004	0.004

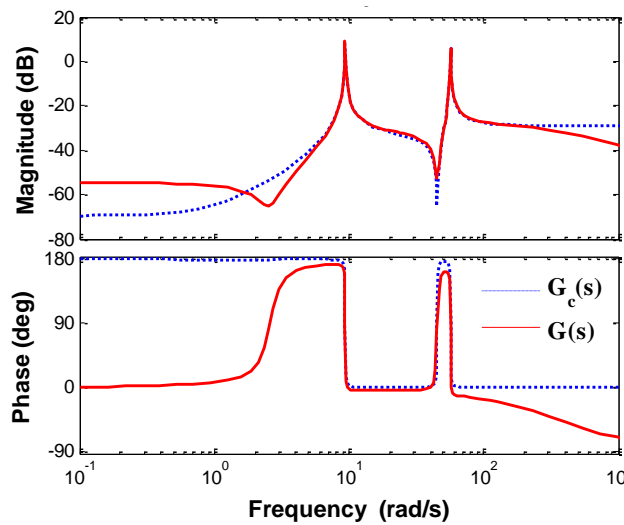


**Figure 5.** Bode diagrams of the identified models.

It can be observed from Table 4 that the first two resonance frequencies of the identified models are 1.48 and 9.06 Hz, which are nearly the same as the results obtained from the measured frequency response in Figure 4. Meanwhile, the two identified models have nearly the same damping ratios for the first two modes. Bode diagrams of the two identified models have similar characteristics nearby the resonance frequencies, as shown in Figure 5. The values of the zeros and poles of the two models are listed in Table 5 based on the ascending order of the image parts. Their locations in the two models are also given in Figure 6.

**Table 5.** Comparison of poles and zeros for the identified models.

Model $G(s)$		Model $G_c(s)$	
Poles	Zeros	Poles	Zeros
$-0.21 - 56.9i$	$-0.79 - 45.21i$	$-0.20 - 56.9i$	$-0.20 - 44.9i$
$-0.036 - 9.33i$	$-0.36 - 2.55i$	$-0.036 - 9.33i$	$-1.19$
$-355.45$	-	-	-
$-0.036 + 9.33i$	$-0.36 + 2.55i$	$-0.036 + 9.33i$	$1.12$
$-0.21 + 56.9i$	$-0.79 + 45.21i$	$-0.20 + 56.9i$	$-0.20 - 44.9i$

It is worth noting that the locations of the poles of the two identified models coincide highly, while the locations of the zeros of the two identified models are totally different, which is because the locations of the zeros are distorted due to the omission of the higher modes, and different system models lead to different relocation of the zeros as depicted before.

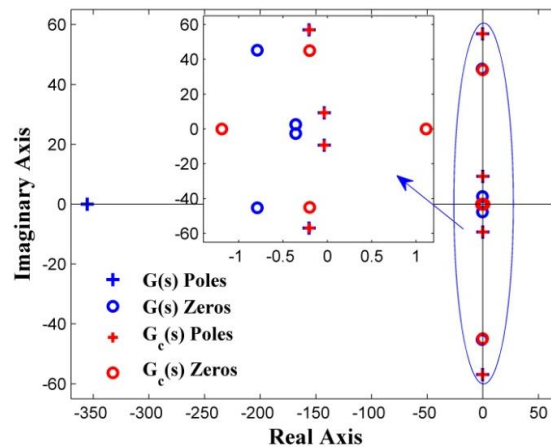


Figure 6. Locations of the zeros and poles.

System responses of the two identified models excited by the same chirp signal are illustrated in Figure 7a,b, both in the time and frequency domains. Besides, the measured system response of the smart structures is also given for comparison. As seen from these figures, system responses of the two identified models are both in good agreement with the experimental response. An excellent match between the identified models and experimental results can be noticed nearby the two resonance frequencies. However, at the beginning period of the chirp excitation ( $t < 1.5$  s), there are some differences between the model  $G_c(s)$  and the measured system responses. It is noticed that system responses of the identified model  $G(s)$  show a better agreement with the experimental responses than that of the model  $G_c(s)$ . As a result, the identified model  $G(s)$  is accurate both in the time and frequency domains.

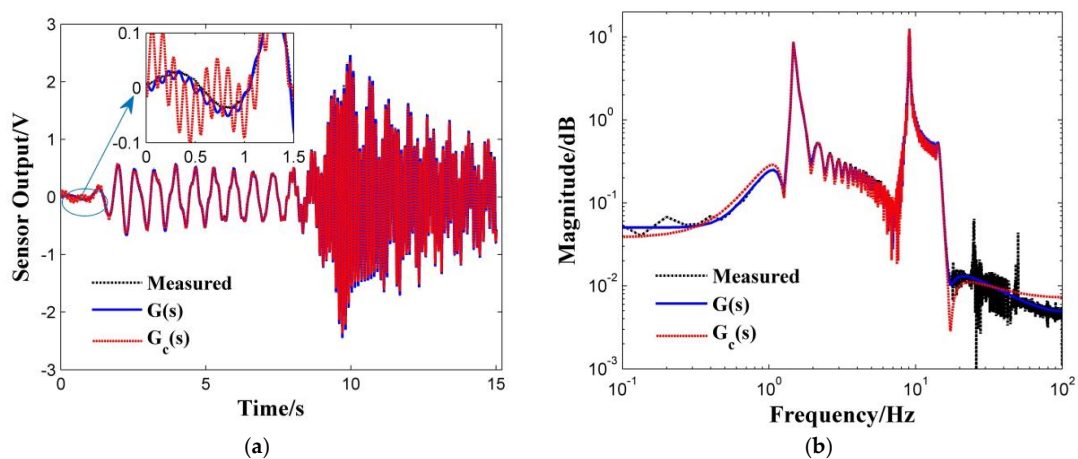
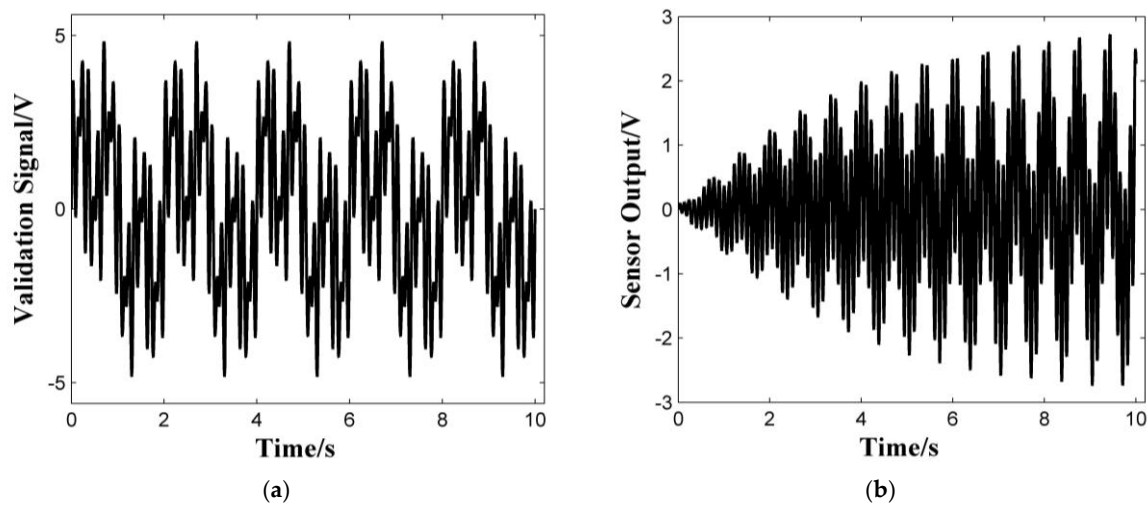


Figure 7. Comparison of system responses with the chirp signal excitation: (a) time responses; and (b) frequency responses.

It should be pointed out that the proposed structure behaves like a collocated system, as shown in Table 4 and Figure 6 [28]. This is because the distance between the strain gauges and the actuators is small, compared to the beam length (the distance between the actuators and sensors is only 63.4 mm, while the length of the beam is 1 m). In addition, since the identified delay time  $\tau$  (0.003 s) is far less than 1 s, it is reasonable that the pure delay element is approximated by a first-order inertia element in Equation (3).

After system model has been identified, it is necessary to validate whether the model is precise enough to represent the real system. The validation experiment is very required since a good match on

one signal alone does not necessarily mean it is well matched on another. For this test, the plant was subjected to a summation excitation of several sinusoidal signals of 1.6 V; their frequencies were at 0.5, 1.5, 6 and 9 Hz, respectively. The time responses for the validation signal are plotted in Figure 8a,b.



**Figure 8.** Time response of the validation excitation and measured output signal: (a) input signal; and (b) sensor output signal.

A comparison between the actual structure and the identified transfer function when subjected to the validation signal is shown in Figure 9a,b. It can be seen that the output signals are very close, thus confirming that the system identification has performed properly. The fitness percentage (FP) between the real output and estimated output was calculated for quantitative comparison, which is defined as Equation (9).

$$FP = 1 - \sqrt{\frac{\sum_{i=1}^N (y_i - \hat{y}_i)^2}{\sum_{i=1}^N y_i^2}} \tag{9}$$

where  $N$  is the number of the acquisition data,  $y_i$  is the measured system response, and  $\hat{y}$  is the estimated response of the identified model. The calculation results are summarized in Table 6.

**Table 6.** Comparison of fitness percentage (FP) of identified models.

Identified Model	Chirp Excitation	Validation Excitation
$G_c(s)$	77.9%	81.4%
$G(s)$	97.2%	90.5%

It is clearly observed from the validation test that the identified model considered in this study performs well. Comparing the FP in Table 5, it is noted that the proposed model  $G(s)$  performs better than the widely used model  $G_c(s)$ . Consequently, the identified model  $G(s)$  with the delay element is chosen to represent the real plant.

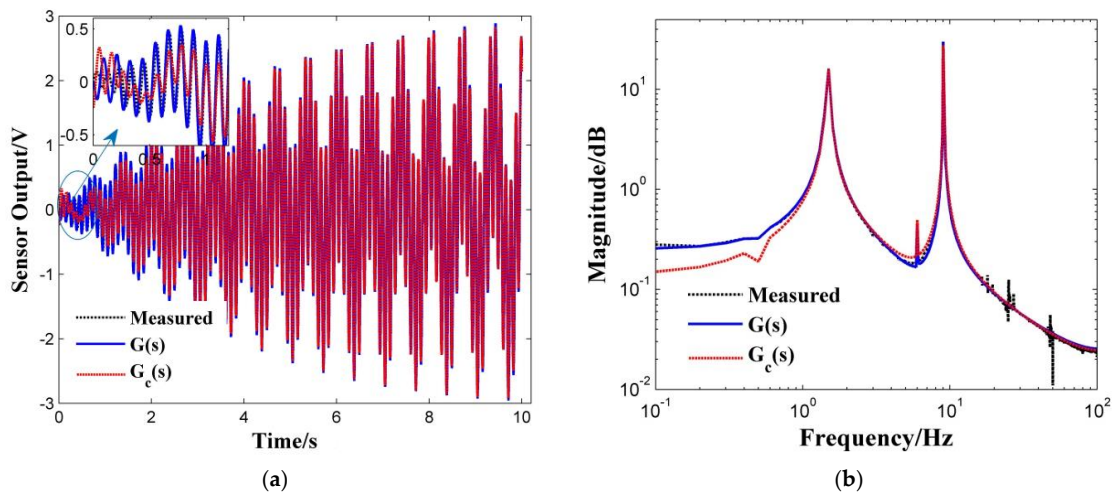


**Figure 9.** Comparison of system responses with the validation signal excitation: (a) time responses; and (b) frequency responses.

#### 4. Controller Design

The poles placement method (PPM) is a well-known approach employed in the feedback control. It offers the flexibility to relocate the dominant poles of the closed loop system to achieve desired performances. PPM is very desirable for feedback control, as the location of the poles corresponds directly to the eigenvalues of the system, which controls the characteristics of the closed loop response [29]. It is known that the poles of symmetric structural systems are complex with real and complex parts. The poles of the proposed smart structure are related to modal damping ratios and natural frequencies by Equation (10)

$$\begin{cases} \lambda_{1,2} = -\zeta_1\omega_1 \pm j\omega_1\sqrt{1-\zeta_1^2} = -\zeta_1\omega_1 \pm j\omega_{d1} \\ \lambda_{3,4} = -\zeta_2\omega_2 \pm j\omega_2\sqrt{1-\zeta_2^2} = -\zeta_2\omega_2 \pm j\omega_{d2} \end{cases} \quad (10)$$

Except the pole corresponding to the inertia element of the identified model  $G(s)$ , the locations of the poles corresponding to the first two modes are plotted in Figure 10.

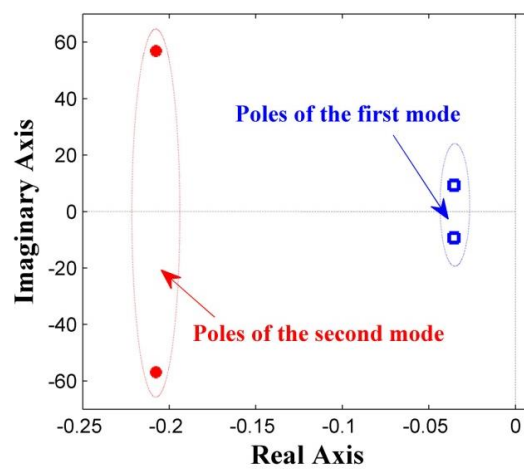


**Figure 10.** Locations of poles corresponding to the first two modes.

Mathematically, if the dominant complex-conjugate poles lie close to the imaginary axis, the system transient response exhibits excessive oscillations and delays slowly. Therefore, to guarantee

fast delay response characteristics, it is necessary to place the closed-loop poles in a particular region far away from the imaginary axis. It can be observed from Figure 10 that both the two pairs of poles locate fairly close to the imaginary axis. Thus, both the two pairs of poles need to be relocated to get a better performance of the system [30].

Compared with the polynomial form, the state space approach is more convenient in designing the controller. As it offers the designer to select  $n$  independent gains for a system, the arbitrarily desired poles is achieved. The state space representation of the system is written as Equation (11)

$$\begin{aligned} \dot{x}(t) &= Ax(t) + Bu(t) \\ y(t) &= Cx(t) + Du(t) \end{aligned} \tag{11}$$

where  $y(t)$  is the output vector, in our case is the voltage output of strain sensors, and  $u(t)$  is the input vector, which is the pre-amplified voltage to the piezoelectric actuators.  $x(t)$ ,  $A$ ,  $B$ ,  $C$  and  $D$  are the state variable vector, state matrix, control matrix, output matrix and direct transfer matrix, respectively. Those parameters are defined as

$$x(t) = \begin{bmatrix} x_1 \\ \vdots \\ x_i \\ \vdots \\ x_n \end{bmatrix} = \begin{bmatrix} \dot{x}_2 + p_1 y(t) - q_1 u(t) \\ \vdots \\ \frac{dx_{i+1}(t)}{dt} + p_i y(t) - q_i u(t) \\ \vdots \\ y(t) \end{bmatrix}, A = \begin{bmatrix} 0 & 0 & \dots & 0 & -p_0 \\ 1 & 0 & \dots & 0 & -p_1 \\ 0 & 1 & \dots & 0 & -p_2 \\ \vdots & \vdots & \vdots & \vdots & \vdots \\ 0 & 0 & \dots & 1 & -p_{n-1} \end{bmatrix}, B = \begin{bmatrix} q_0 \\ q_1 \\ q_2 \\ \vdots \\ q_{n-1} \end{bmatrix}, C = \begin{bmatrix} 0 \\ 0 \\ 0 \\ \vdots \\ 1 \end{bmatrix}^T, D = 0 \tag{12}$$

where  $n$  is the degree of the denominator of the identified model  $G(s)$ , and in our case is 5.  $p_n, p_{n-1}, \dots, p_1$  and  $p_0$  are the coefficients of the denominator of  $G(s)$  in descending powers of  $s$ .  $q_n, q_{n-1}, \dots, q_1$  and  $q_0$  are the coefficients of the numerator of  $G(s)$ .

The state space equations must be controllable in order to implement the PPM. Thus, system observability and controllability matrices are calculated to ensure all the states are controllable and observable. Once those are determined, poles of the closed loop system could be placed at any desired location by means of state feedback through an appropriate state feedback gain matrix. The feedback control  $u(t)$  can be defined as Equation (13)

$$u(t) = -Kx(t) \tag{13}$$

where  $K$  is the state feedback gain matrix. Substituting Equation (13) into Equation (11) gives Equation (14)

$$\dot{x}(t) = (A - BK)x(t) \tag{14}$$

The eigenvalues of matrix  $(A - BK)$  are the closed loop poles of the controlled system, which determine the closed loop performance of the system. If the locations of the desired poles are determined, the feedback gain matrix can be solved using Equation (15)

$$|sI - (A - BK)| = \prod_{i=1}^g (s - p_i) \tag{15}$$

where  $p_i$  is the desired closed loop poles,  $g$  is the poles number.

For effective vibration suppression, it is necessary to choose the closed loop poles appropriately. In practice, if the desired closed loop poles are placed far from the left of the imaginary axis, the voltage delivered by the controller might exceed the actuator limits, thus possibly destabilizes the closed loop system; Furthermore, the generated voltage may oscillate too fast in order to control the system, and a noise amplification will be caused, which leads to a possible excitation of the high frequency modes of the system. Consequently, the spillover effect is unavoidable. On the other hand, a close location of closed loop poles may lead to a slow closed loop response. Therefore, a compromise needs to be found between the response time and control force.

To achieve the desired damping characteristics of the target modes, without affecting the natural frequencies of the structure, the best solution is to adjust only the real part of the dominant poles. As it is known, the dynamic response of a second order system has no vibration and achieves a stable state in a short time when the damping ratio is 0.707. Thus, the optimal locations of the desired poles can be attained when the closed loop damping ratio is set to be 0.707. The basic idea of this method is illustrated in Figure 11. The comparisons between the relocated closed loop and open loop poles are listed in Table 7.

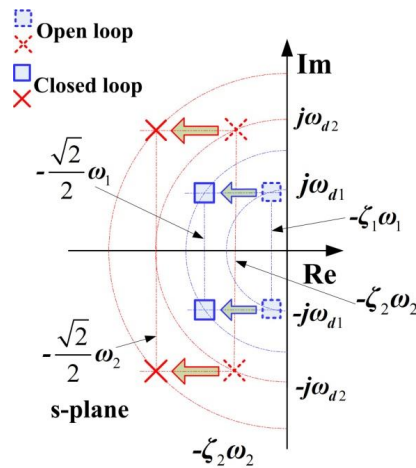


Figure 11. Optimal locations of the closed loop poles.

Table 7. Comparisons between the closed loop and open loop poles.

Open Loop Poles	Open Loop Damping Ratio	Closed Loop Poles	Close Loop Damping Ratio
$-0.036 \pm 9.33i$	0.004	$-6.59 \pm 9.33i$	0.707
$-0.21 \pm 56.9i$	0.004	$-40.23 \pm 56.9i$	0.707

### 5. Simulations

To evaluate the effectiveness of the proposed controller, simulations of system response in the closed loop were performed with the above derived transfer function  $G(s)$ . The excitation signal was a summation of the two sinusoidal signals of modal frequencies 1.5 Hz and 9 Hz for a period of 10 s at 0.5 V. A saturation block with limits of  $\pm 5$  V was incorporated to limit the control effort, as it would be in implementation. The simulated time responses for the open and closed loop system in a total period of 40 s are shown in Figure 12.

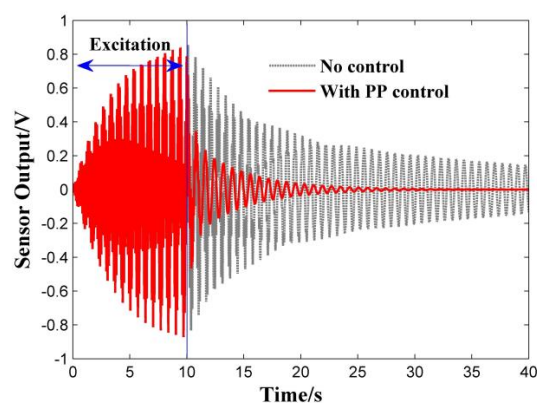


Figure 12. Simulated time responses for open and closed loop system. PP: Poles Placement.

As plotted in Figure 12, the excited vibrations for the open loop system take more than 30 s to eliminate, while with the poles placement controller, the system vibrations die down in less than 15 s. Obviously, system vibrations are effectively suppressed. Furthermore, two sets of optional locations for the closed loop poles, as given in Table 8, are chosen to verify the effectiveness of the proposed controller.

**Table 8.** Comparisons of optional locations for closed loop poles.

Optional Location	Closed-Loop Poles	Damping Ratio
Closer location	$-3.73 \pm 9.33i$ $-22.76 \pm 56.9i$	0.4
Optimal location	$-6.59 \pm 9.33i$ $-40.23 \pm 56.9i$	0.707
Further location	$-7.93 \pm 9.33i$	0.85

After the locations of the desired poles are determined, Equation (15) can be rewritten as

$$|sI - (A - BK)| = (s - p_d) \prod_{i=1}^2 (s - p_i)(s - \hat{p}_i) \tag{16}$$

where  $p_i$  and  $\hat{p}_i$  are the complex-conjugate poles, and  $p_d$  is the pole corresponding to the first-order inertia element. Then, the feedback gain matrix can be solved using Equation (16).

Simulation results with different locations of closed loop poles are illustrated in Figure 13a–d. It can be seen that a further location of the closed loop poles leads to a better control performance, but a severer spillover phenomenon is caused as shown in Figure 13b. On the other hand, the spillover phenomenon is avoided with a closer location of the closed loop poles as plotted in Figure 13c. However, the effectiveness of the controller decreases unavoidably. It can be seen more clearly from the power spectral density plot Figure 13d, there are excitation energy peaks at 50 Hz for the cases  $\zeta = 0.707$  and 0.85. Therefore, the spillover phenomenon appears as the peaks are outside the desired frequency bandwidth.

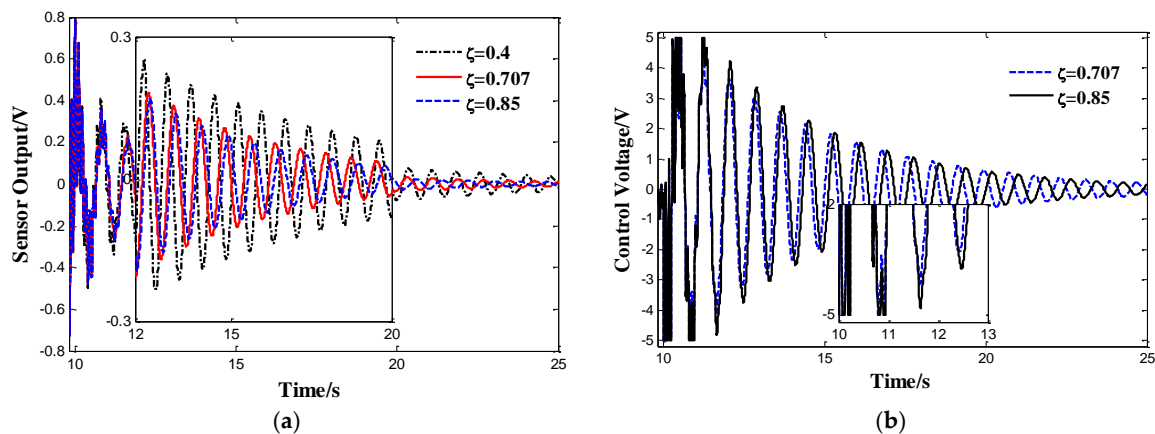


**Figure 13.** Cont.

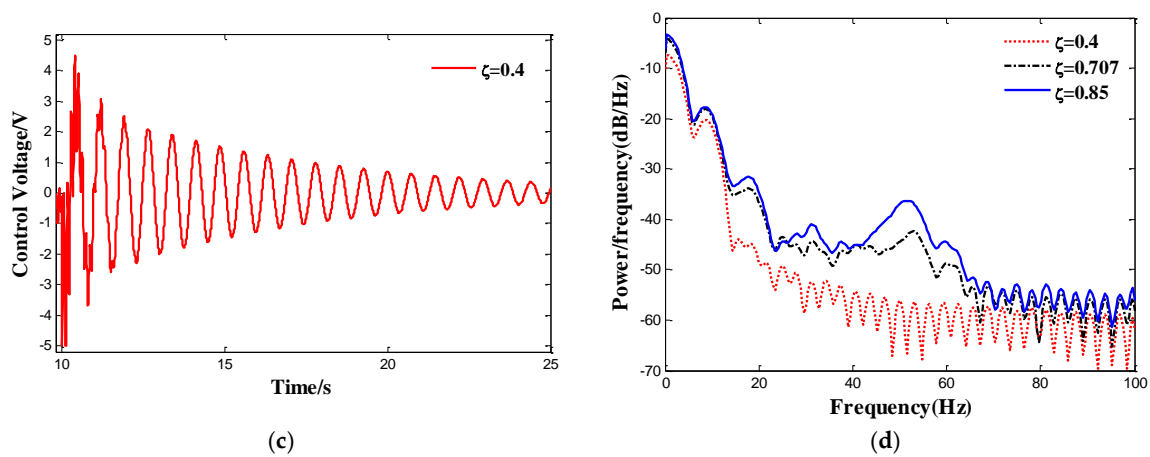


**Figure 13.** Simulation results with different locations of the closed loop poles: (a) time response of the closed loop system; (b) control voltage of PZT actuators; (c) control voltage of PZT actuators; and (d) power spectral density of the control voltage.

### 6. Experiments

The identified model combined with the proposed controller was implemented on the experimental setup. The controller was tested in the real time data acquisition system with the same sampling frequency of 200 Hz. The experimental setup was excited using the same excitation signal used in simulation. The open loop test was conducted to view the results in the absence of the controller. The comparisons of the free vibrations (without control) results between simulation and experiment are shown in Figure 14. It is clear that the experimental results are in good agreement with simulation for the open loop test. It should be pointed out that the amplitude of the time response in simulation is a little larger than that in experiment. This is because the identified model  $G(s)$  corrects for the neglected modes.

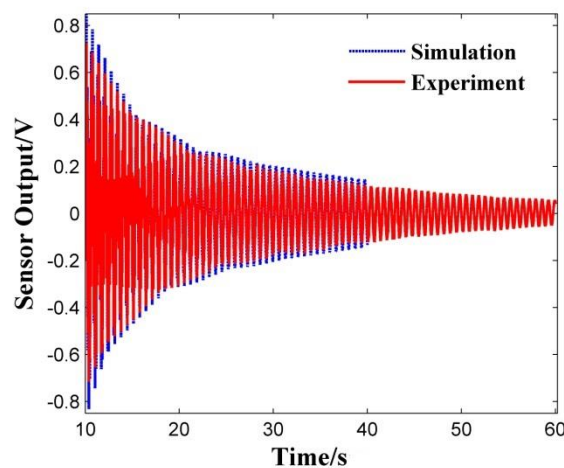


**Figure 14.** Comparisons of free vibration results between simulation and experiment.

In addition, the tip displacement measured by the laser displacement sensor is plotted in Figure 15. It can be seen that the uncontrolled tip displacement of the manipulator still has an amplitude of 0.25 mm, after a damping period of 60 s. The time taken for the vibration to settle down is so long that vibration control must be carried out to accelerate this process.

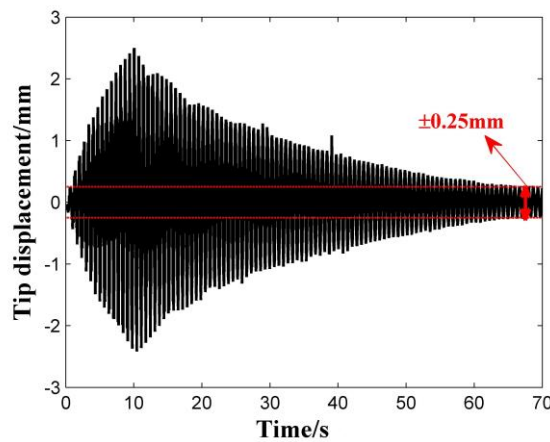


Figure 15. Tip displacement measured by the laser displacement sensor.

Next, the controller with the optimal locations of desired poles was implemented. The closed loop time responses with the PPM are shown in Figure 16a. It can be seen that the system vibrations are well suppressed with the proposed controller, and the damping period of the vibration response is shortened significantly. Furthermore, the power spectral density comparisons for 10 seconds(s) to 25 s are shown in Figure 16b. Compared with the responses of the open loop, the measured magnitude at the first resonant frequency drops from 5.6 decibel (dB) to 4.1 dB, and a drop of 2.3 dB is observed for the second resonant frequency. Evidently, substantial drops are observed at the first two resonant frequencies. Moreover, the closed loop time responses for the simulated and experimental results match closely, as shown in Figure 17. It is noted that the control efficiency in experiment is a little better than that in simulation. This is because the amplitude of time response in simulation is a little larger than that in experiment as shown in Figure 14. The measured tip displacement is shown in Figure 18. After a damping period of 13 s, the amplitude of the controlled tip displacement reduces to 0.05 mm. Thus, a quick vibration convergence is achieved with the proposed controller.

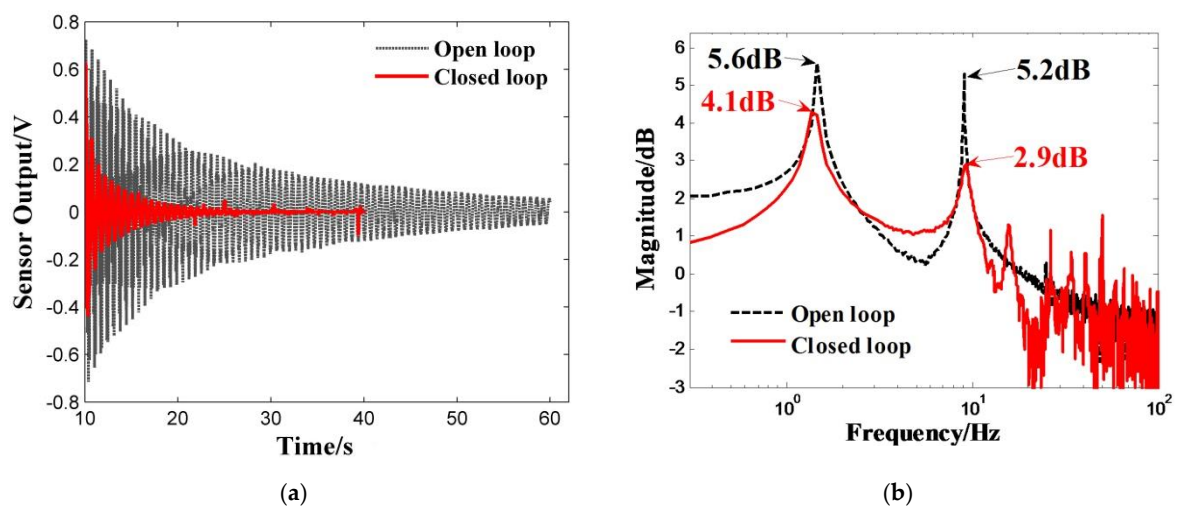


Figure 16. Comparisons of experimental responses between the open and closed loop: (a) time response; and (b) power spectral density.

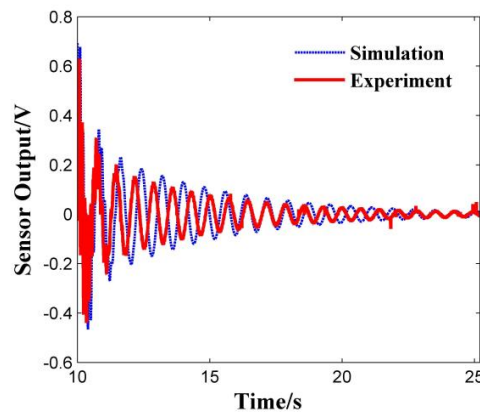


Figure 17. Comparisons of the closed loop time responses.

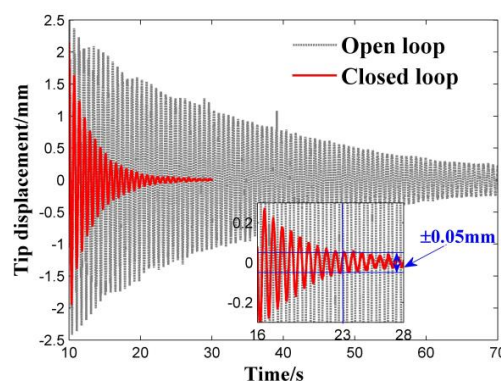


Figure 18. Comparisons of the measured tip displacement.

To further evaluate the performance of the controller, the same structure was subjected to an external disturbance by the electromagnetic vibrator (EMV). The controller is switched on when the structure is excited by the vibrator. The open loop (without control) and closed loop (with the controller) time responses are shown in Figure 19a. In the absence of the controller, the uncontrolled response measured by the strain sensors still has an amplitude of 0.14 V after a damping period of 50 s, while now is suppressed to 0.05 V within 9 s, and the power spectral density comparisons for a period of 25 s are presented in Figure 19b.

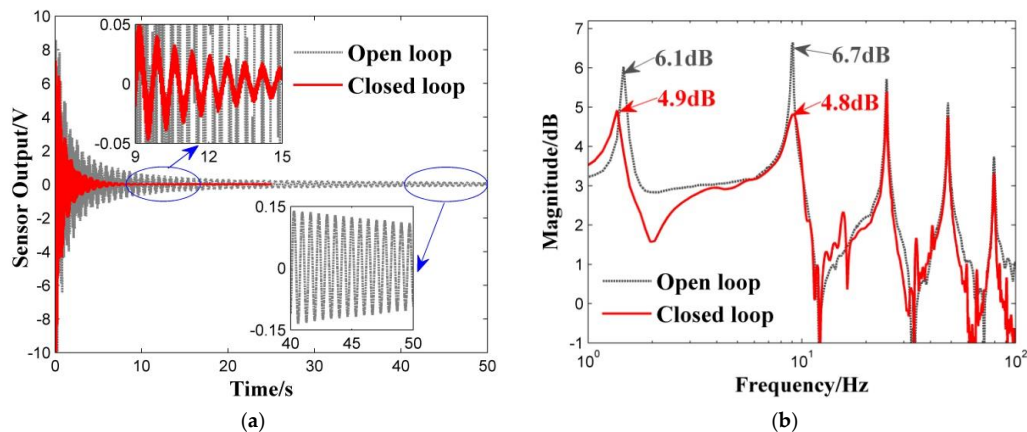


Figure 19. Comparisons of experimental responses excited by the electromagnetic vibrator (EMV): (a) time response; and (b) power spectral density.

It is noticed that the first two vibration modes are well suppressed. This is expected to happen since the first two modes, corresponding to the first two pairs of dominant poles, are the ones that are mostly needed to be diminished. Moreover, it is also interesting to notice from Figure 19b that the three higher modes (the third, fourth and fifth peaks), excited by the impulse excitation of the EMV, also experience a small attenuation. Even though the corresponding poles have not been changed, this might be the influence of the first two pairs of poles that have been relocated. As the three higher vibration modes have fast convergence speed in the time domain, they are not dominant to affect the system response. The induced vibrations die down very quickly with the proposed controller as compared in Figure 20.

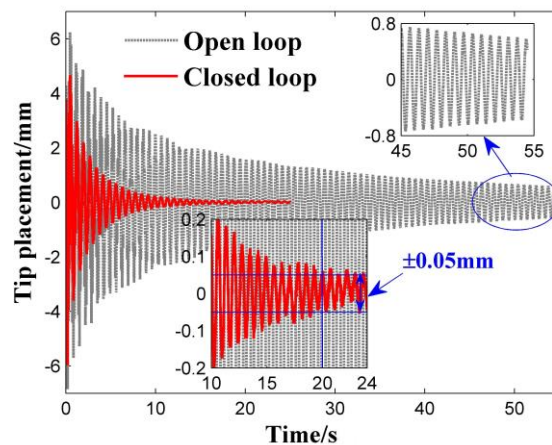


Figure 20. Comparisons of measured tip displacement excited by the EMV.

The amplitude of the controlled tip displacement reduces to 0.05 mm after a damping period of 13 s, while the damping period takes more than 60 s without the controller. Besides, it is necessary to notice as the peak value of the measured vibration response exceeds the range of the A/D board ( $\pm 10$  V) as plotted in Figure 19a; control saturation of actuators is inevitable. The control voltage applied on actuators is depicted in Figure 21.

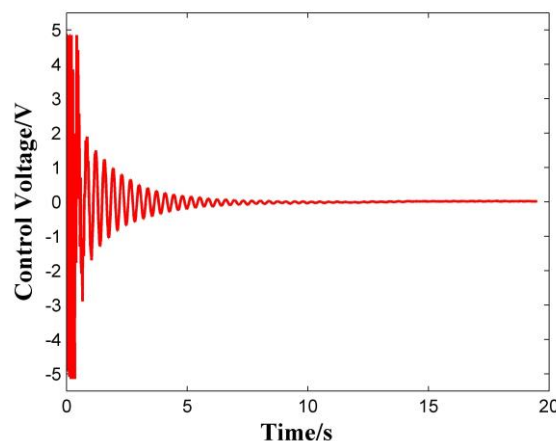
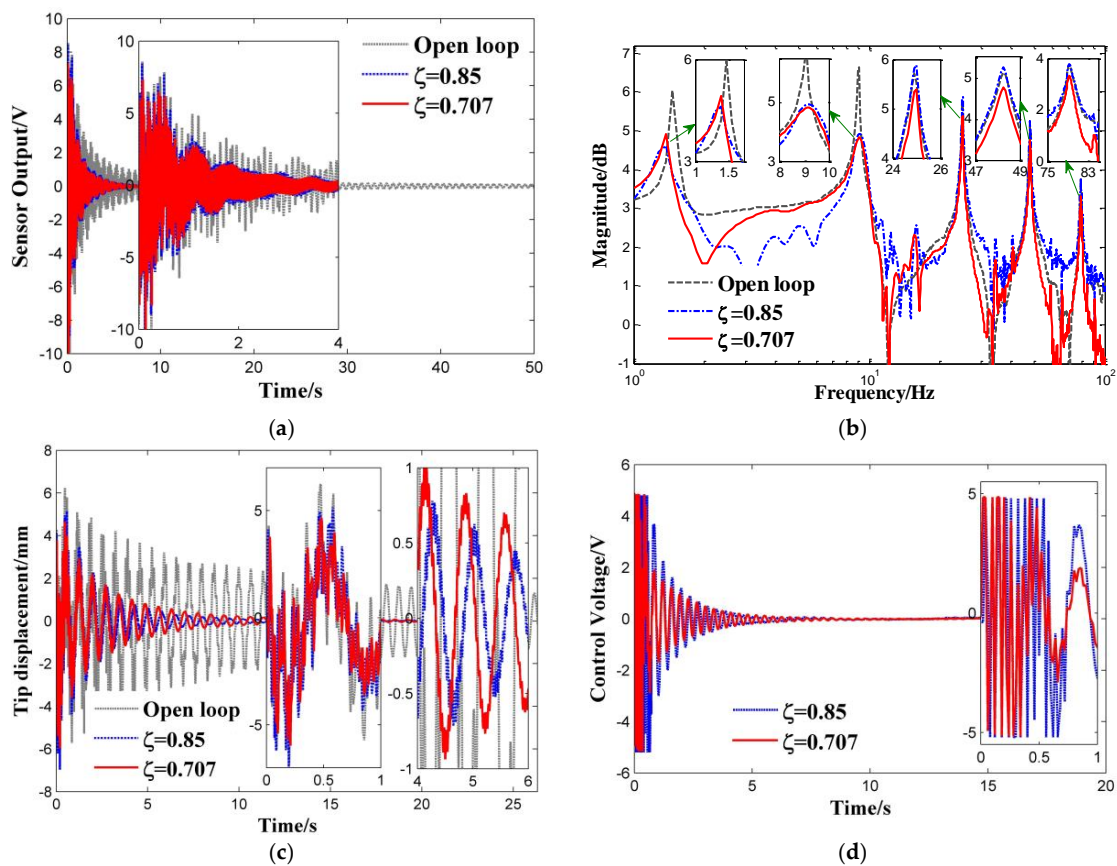


Figure 21. Control voltage applied on actuators.

Finally, experimental results of the poles placement controller with different locations of the closed loop poles are compared in Figure 22a–d. Significant attenuation of measured time responses measured by the strain sensors can be seen for the two cases, namely the further location of poles with damping ratio 0.85 ( $-48.37 \pm 56.9i$ , and  $-7.93 \pm 9.33i$ ) and the optimal location of poles with damping ratio 0.707 ( $-40.23 \pm 56.9i$ , and  $-6.59 \pm 9.33i$ ).



**Figure 22.** Comparisons of experimental results with different locations of poles: (a) measured time response by strain sensors; (b) power spectral density; (c) measured tip displacement; and (d) control voltage applied on the actuators.

However, it is important to point out that the measured time responses with the further location of poles decays a little slower than that with the optimal location of poles in Figure 22a. The experimental results show the control effectiveness reduces with a further location of poles, which is different from simulations. In the case of further location of poles, it is observed that vibration responses of the first two modes are well suppressed, and a larger attenuation of the first mode is achieved in Figure 22b, compared with the optimal case. However, peaks corresponding to the other three higher modes (the third, fourth and fifth peaks) have larger amplitudes than that in the open loop case. All these can be attributed to the fact that the desired closed loop poles are placed too far from the imaginary axis; hence, the control voltage delivered by the controller severely exceeds the system limits, which leads to a severe control saturation phenomenon as demonstrated in Figure 22d. Furthermore, the spillover effect is caused by the control saturation, and vibrations of the higher modes are excited. Those results are further illustrated by the measured vibration response of the beam tip in Figure 22c. During the beginning period (0–1 s), vibrations of the higher modes are excited due to the severe spillover effect, thus the peak values of tip displacement with the further location of poles are slightly larger than that with the optimal case. As vibrations of the higher modes converge quickly in the time domain, the spillover effect disappears during the periods of 4–6 s, and the control force of the actuators is mainly used to deal with vibrations of the first two modes. Correspondingly, the control effectiveness with the further location of poles is better than that with the optimal case in the period of 4–6 s.

In summary, locations of the closed loop poles must be carefully determined to implement the poles placement controller. The effectiveness of the optimal multi-poles placement method is validated by experiments. Multi-mode vibrations of the smart flexible manipulator are well suppressed with the proposed controller.

## 7. Conclusions

Experimental identification and multi-mode vibration suppression of a smart flexible manipulator bonded with piezoelectric actuators and strain sensors are conducted in this paper. A reduced order transfer function representing the physical system is proposed, and a first-order inertia element is added to the model for experimental identification. An optimal multi-poles placement controller is proposed and implemented on the structure. Both comparative simulated and experimental results validate the effectiveness and feasibility of the proposed controller. The conclusions of this study can be summarized as follows:

To describe the smart flexible manipulator system, a reduced order transfer function model with relocated zeros compensating for the neglect of higher modes is proposed. A first-order inertia element is added to the model for system identification. Comparative results show the identified model matches closely with the experimental results both in the time and frequency domains, and a fit of 97.2% is achieved in the identification results. The validation test with an excitation of several sinusoidal signals further validated the excellent performance of the proposed model.

An optimal multi-poles placement controller is designed and implemented on the structure. A method where the move distance of the closed loop poles is the shortest is proposed, and the optimal locations of the closed loop poles are determined at the best damping ratio 0.707. Compared with different locations of poles, the best performance of the optimal locations of poles is demonstrated by simulations. Experimental results show vibrations of the first two modes of the manipulator are significantly diminished as expected. Moreover, vibrations of the higher modes are also slightly suppressed with the proposed controller. In addition, if a further location of poles is chosen, the spillover effect will be caused due to the control saturation of actuators, and vibrations of the higher modes will be excited. Consequently, the best performance for the optimal locations of the closed loop poles is validated, and the effectiveness and feasibility of the proposed controller are demonstrated.

**Acknowledgments:** This work was supported by the National Natural Science Foundation of China (No. 51505238 and 51375433) and Zhejiang Provincial Natural Science Foundation of China (No. LQ15E050002). The authors would also like to thank the support of Kuan Cheng Wong Magna Fund in Ningbo University, Ningbo, China.

**Author Contributions:** Yanding Wei conceived the experiments; Jiangjiang Liao performed the experiments. Yiling Yang analyzed the data; Guoping Li Set up the experiments; and Junqiang Lou wrote the paper.

**Conflicts of Interest:** The authors declare no conflict of interest.

## References

1. Zhao, Z.L.; Qiu, Z.C.; Zhang, X.M. Vibration control of a pneumatic driven piezoelectric flexible manipulator using self-organizing map based multiple models. *Mech. Syst. Signal Process.* **2016**, *70–71*, 345–372. [[CrossRef](#)]
2. Xu, Z.; Shan, X.; Chen, D.; Xie, T. A Novel Tunable Multi-Frequency Hybrid Vibration Energy Harvester Using Piezoelectric and Electromagnetic Conversion Mechanisms. *Appl. Sci.* **2016**, *6*, 10. [[CrossRef](#)]
3. Lou, J.Q.; Wei, Y.D.; Yang, Y.L.; Xie, F.R. Hybrid PD and effective multi-mode positive position feedback control for slewing and vibration suppression of a smart flexible manipulator. *Smart Mater. Struct.* **2015**, *24*, 035007. [[CrossRef](#)]
4. Sethi, V.; Franchek, M.A.; Song, G.B. Active multimodal vibration suppression of a flexible structure with piezoceramic sensor and actuator by using loop shaping. *J. Vib. Control* **2011**, *17*, 1994–2006. [[CrossRef](#)]
5. Jonathan, B.; Ramón, T.J.; Vicente, F.; Hebertt, S.R. Adaptive Controller for Single-Link Flexible Manipulators Based on Algebraic Identification and Generalized Proportional Integral Control. *IEEE Trans. Syst. Man Cybern. B* **2009**, *39*, 735–751.
6. Tornabene, F.; Fantuzzi, N.; Bacciocchi, M.; Reddy, J. An Equivalent Layer-Wise Approach for the Free Vibration Analysis of Thick and Thin Laminated and Sandwich Shells. *Appl. Sci.* **2016**, *7*, 17. [[CrossRef](#)]
7. Saad, M.S.; Jamaluddin, H.; Darus, I.Z.M. Active vibration control of a flexible beam using system identification and controller tuning by evolutionary algorithm. *J. Vib. Control* **2013**, *21*, 2027–2042. [[CrossRef](#)]
8. Bu, X.Z.; Ye, L.; Su, Z.Q.; Wang, C.H. Active control of a flexible smart beam using a system identification technique based on ARMAX. *Smart Mater. Struct.* **2003**, *12*, 845–850. [[CrossRef](#)]

9. Abreu, G.L.C.M.; Conceicao, S.M.; Brennan, M.J.; Alves, M.T.S. System Identification and Active Vibration Control of a Flexible Structure. *J. Braz. Soc. Mech. Sci. Eng.* **2012**, *34*, 386–392. [[CrossRef](#)]
10. Tavakolpour, A.R.; Darus, I.Z.M.; Tokhi, O.; Mailah, M. Genetic algorithm-based identification of transfer function parameters for a rectangular flexible plate system. *Eng. Appl. Artif. Intell.* **2010**, *23*, 1388–1397. [[CrossRef](#)]
11. Afshari, S.S.; Nobahari, H.; Kordkheili, S.A.H. Experimental Parametric Identification of a Flexible Beam Using Piezoelectric Sensors and Actuators. *Shock Vib.* **2014**, *2014*, 718140.
12. Pradhan, S.K.; Subudhi, B. Nonlinear Adaptive Model Predictive Controller for a Flexible Manipulator: An Experimental Study. *IEEE Trans. Control Syst. Technol.* **2014**, *22*, 1754–1768. [[CrossRef](#)]
13. San-Millan, A.; Feliu, V. A Fast Online Estimator of the Two Main Vibration Modes of Flexible Structures from Biased and Noisy Measurements. *IEEE-ASME Trans. Mech.* **2015**, *20*, 93–104. [[CrossRef](#)]
14. Qiu, Z.C.; Wu, H.X.; Ye, C.D. Acceleration sensors based modal identification and active vibration control of flexible smart cantilever plate. *Aerosp. Sci Technol.* **2009**, *13*, 277–290. [[CrossRef](#)]
15. Bhikkaji, B.; Moheimani, S.O.R.; Petersen, I.R.A. Negative Imaginary Approach to Modeling and Control of a Collocated Structure. *IEEE-ASME Trans. Mech.* **2012**, *17*, 1–11. [[CrossRef](#)]
16. Ahmadizadeh, S.; Montazeri, A.; Poshtan, J. Design of minimax-linear quadratic Gaussian controller using the frequency domain subspace identified model of flexible plate. *J. Vib. Control* **2015**, *21*, 1115–1143. [[CrossRef](#)]
17. Orszulik, R.R.; Shan, J.J. Experimental study on active vibration control using genetic algorithm-based system identification and optimized positive position feedback. *Smart Mater. Struct.* **2012**, *21*, 125014. [[CrossRef](#)]
18. Bandopadhyaya, D.; Njuguna, J. A Study on the Effects of Kalman Filter on Performance of IPMC-Based Active Vibration Control Scheme. *IEEE Trans. Control Syst. Technol.* **2010**, *18*, 1315–1324. [[CrossRef](#)]
19. Kumar, R. Efficient Active Vibration Control of Smart Structures with Modified Positive Position Feedback Control Using Pattern Search Methods in the Presence of Instrumentation Phase Lead and Lag. *J. Dyn. Syst. Trans. ASME* **2013**, *135*, 1012–1030. [[CrossRef](#)]
20. Demetriou, D.; Nikitas, N. A Novel Hybrid Semi-Active Mass Damper Configuration for Structural Applications. *Appl. Sci.* **2016**, *6*, 397. [[CrossRef](#)]
21. Abdelaziz, T.H.S. Parametric eigenstructure assignment using state-derivative feedback for linear systems. *J. Vib. Control* **2012**, *18*, 1809–1827. [[CrossRef](#)]
22. Sethi, V.; Song, G.B. Pole-Placement Vibration Control of a Flexible Composite I-beam using Piezoceramic Sensors and Actuators. *J. Thermoplast. Compos.* **2006**, *19*, 293–307. [[CrossRef](#)]
23. Sethi, V.; Song, G.B. Multimodal Vibration Control of a Flexible Structure using Piezoceramic Sensor and Actuator. *J. Intell. Mater. Syst. Struct.* **2008**, *19*, 573–582. [[CrossRef](#)]
24. Tehrani, M.G.; Mottershead, J.E.; Shenton, A.T.; Ram, Y.M. Robust pole placement in structures by the method of receptances. *Mech. Syst. Signal Process.* **2011**, *25*, 112–122. [[CrossRef](#)]
25. Gordon, D.J.; Erkorkmaz, K. Accurate control of ball screw drives using pole-placement vibration damping and a novel trajectory prefilter. *Precis. Eng.* **2013**, *37*, 308–322. [[CrossRef](#)]
26. Tehrani, M.G.; Elliott, R.N.R.; Mottershead, J.E. Partial pole placement in structures by the method of receptances: Theory and experiments. *J. Sound Vib.* **2010**, *329*, 5017–5035. [[CrossRef](#)]
27. Orszulik, R.R.; Shan, J.J. Active vibration control using genetic algorithm-based system identification and positive position feedback. *Smart Mater. Struct.* **2012**, *21*, 055002. [[CrossRef](#)]
28. Obrzut, T.M. *Non-Collocation Problems in Dynamics and Control of Mechanical System*; Cleveland State University: Cleveland, OH, USA, 2009.
29. Mottershead, J.E.; Tehrani, G.M.; James, S.; Court, P. Active vibration control experiments on an AgustaWestland W30 helicopter airframe. *Mech. Eng. Sci.* **2012**, *226*, 1504–1516. [[CrossRef](#)]
30. John, E.; Mottershead, J.E.; Tehrani, M.G.; James, S.; Ramb, Y.M. Active vibration suppression by pole-zero placement using measured receptances. *J. Sound Vib.* **2008**, *311*, 1391–1408.

